

# AN ANGULAR FREQUENCY DOMAIN METRIC FOR THE EVALUATION OF WAVE FIELD RENDERING TECHNIQUES

A. Canclini<sup>§</sup>, P. Annibale<sup>†</sup>, F. Antonacci<sup>§</sup>, A. Sarti<sup>§</sup>, R. Rabenstein<sup>†</sup>, and S. Tubaro<sup>§</sup>

<sup>§</sup> Dipartimento di Elettronica ed Informazione (DEI)  
Politecnico di Milano, 20133 Milano, Italy

<sup>†</sup> Chair of Multimedia Communications and Signal Processing (LMS)  
University Erlangen-Nuremberg, Cauerstr. 7, 91058 Erlangen, Germany

## ABSTRACT

Spatial sound rendering techniques are based on established theoretical frameworks. The theoretical wave field predicted by the underlying of a specific rendering technique is an approximation of the desired ideal wave field. Moreover the practical implementations require often compromises which cause an additional deviation of the rendered wave field from the desired one. To assess these deviations, metrics are devised which quantify the difference of two wave fields. Typically they rely on the comparison of the wave fields at a discrete set of positions in the area of interest (discrete-space metric). In this paper a novel metric is proposed which is formulated in the angular frequency domain. It expresses the difference of two wave fields in terms of their Fourier series angular coefficients. It is efficient since it avoids the spatial summation over a discrete grid in the area of interest, moreover it is flexible since it considers a weighting function to focus the evaluation on specific regions of spatial and temporal frequencies. After a theoretical treatment such a metric is computed for simulated and measured data and compared with a discrete-space metric. The comparison shows that the new metric yields results which allow a flexible assessment of the characteristics of the rendering techniques.

## 1. INTRODUCTION

Spatial sound rendering techniques like Wave Field Synthesis (WFS), Higher-Order Ambisonics (HOA), Vector Based Amplitude Panning (VBAP) are based on established theoretical frameworks. Necessarily the theoretical wave field predicted by the underlying theory of a specific rendering technique is an approximation of the desired wave field and presents to some extent a deviation from it. Such a deviation may be evaluated by comparing the analytic description of the desired and theoretical wave fields, where the latter is derived under ideal conditions (i.e. the loudspeaker array of the reproduction system is generally described by a distribution of ideal point sources and the acoustic chamber is considered as perfectly anechoic). Examples of theoretical comparisons between rendering techniques can be found in [1, 2].

However the implementation on real reproduction systems involves a number of non-idealities of both loudspeakers and environment which alters further the quality of the rendered wave field with respect to the desired one. In order

to evaluate this additional degradation, methodologies for accurately measuring the rendered wave field inside the listening area are required. Finally to assess the performance of different rendering techniques it is necessary to define metrics suitable to quantify the mentioned deviations in a concise fashion.

These issues have been already tackled by the authors in [3], where a well-established technique for the measurement of a wave field is employed. The rendered wave field is sampled over a circle with a pair of rotating microphones, then the rendered wave field inside and outside the circle is extrapolated by means of the circular harmonic decomposition [4]. In order to compare theoretical and measured wave fields with the desired one, in [3] a discrete-space evaluation metric based on the spatial Root Mean Square Error (RMSE) is proposed. Such a metric is computed for simulated and measured data and it is shown that it captures the subtle differences of theoretical and rendered wave fields even in controlled environments (quasi-anechoic chamber and high-quality loudspeakers).

This paper presents an alternate metric in the angular frequency domain for evaluating the ability of a wave field rendering technique to reproduce a desired sound field. Such a metric is a prerequisite for a subsequent perceptual evaluation which is topic of ongoing research. It expresses the RMSE of two wave fields in terms of their Fourier series angular coefficients. Such a novel metric is computed for the same data considered in [3] and it is shown that the new metric yields results which allow a flexible assessment of the characteristics of the rendering techniques. The paper is structured as follows. Sec. 2 briefly reviews the description of a wave field in spherical and polar coordinates and explains the role of the Fourier series angular coefficients. It also specifies the concepts of desired, theoretical and measured wave fields. Sec. 3 introduces the idea of an evaluation metric for comparing different wave fields based on the error energy. Sec. 4 shows the derivation of a metric based on the Fourier series angular coefficients, while in Sec. 5 the results obtained with the new metric are compared with the ones from [3]. Finally Sec. 6 draws some conclusions.

## 2. REPRESENTATION OF WAVE FIELDS IN SPHERICAL AND POLAR COORDINATES

### 2.1 3D Spherical Coordinates

The Fourier transform of three-dimensional wave fields with exterior sources can be expressed in spherical coordinates as

The research leading to these results has received funding from the European Community's Seventh Framework Programme (FP7/2007-2013) under grant agreement No. 226007. This paper is the continuation of the work carried out during the visit of the first author at LMS.

sum of spherical harmonic functions  $Y_n^m(\theta, \phi)$

$$P(\omega, \rho, \theta, \phi) = \sum_{n,m} A_{nm}(\omega) j_n\left(\frac{\omega}{c}\rho\right) Y_n^m(\theta, \phi), \quad (1)$$

where  $\omega$  is the temporal frequency,  $\rho$  the radius,  $\theta$  and  $\phi$  are zenith and azimuth angles, respectively and  $j_n\left(\frac{\omega}{c}\rho\right)$  the spherical Bessel functions. Definitions and properties of these functions and of the spherical coordinate system are chosen as in [5]. The radius independent spherical harmonic coefficients  $A_{nm}$  provide an exact representation of 3D wave fields. However they are hard to compute analytically and their determination from measurements is restricted to low orders. Exact determination of high order coefficients from measurements would require high resolution sampling on a sphere (see [6] and references cited there).

Much less involved is the description and the measurement process of two-dimensional wave fields in polar coordinates.

## 2.2 2D Polar Coordinates

A two-dimensional wave field can be represented in polar coordinates with radius  $\rho$  and angle  $\phi$  by a Fourier series with coefficients  $\dot{P}_v(\omega, \rho)$  [7]

$$P(\omega, \rho, \phi) = \sum_{v=-\infty}^{\infty} \dot{P}_v(\omega, \rho) e^{jv\phi} = \sum_{v=-\infty}^{\infty} C_v(\omega) J_v(k\rho) e^{jv\phi}. \quad (2)$$

It is well known that 2D wave fields are described exactly by the circular harmonic coefficients  $C_v(\omega)$ . They are independent of the radius  $\rho$ , which is in turn represented by the Bessel function  $J_v(k\rho)$  with  $k = \omega/c$ . The analytical determination of the circular harmonic coefficients involves an integration with respect to the angle  $\phi$ . Thus they are in general easier to evaluate than the spherical harmonic coefficients which require integration with respect to two angles. They can also be obtained from measurements of real sound fields on a circle. Suitable devices and evaluation methods are described e.g. in [8, 9, 10, 11, 12].

From a practical point of view it is then clear that the 2D approach is more attractive, but the use of a 2D representation for evaluating real 3D wave fields requires further considerations.

## 2.3 Relation between 2D and 3D Representations

The connection between the 2D and 3D representations from Sec. 2.1 and Sec. 2.2 can be established by observing that measuring on a circle is equivalent to sampling the zenith angle  $0 < \theta < \pi$  with only one sample at  $\theta = \frac{\pi}{2}$ . This case is investigated in [8, Sec. 4.4]. The following conclusions can be drawn:

- The coefficients  $A_{nm}$  for the same mode number  $m$  but different value  $n$  cannot be separated (order aliasing).
- An exact reconstruction of 3D wave fields from 2D circular measurements is not possible.
- Nevertheless, circular measurements are very useful for 3D wave fields with certain restrictions (e.g. weak floor and ceiling reflections, etc.).
- In particular, results from circular measurements can be still employed to compare different wave fields. They truly represent a wave field at the measurement positions

but should not be used to extrapolate a general wave field to other positions in space unless significant a priori information is available (see [8]).

Considering the above reasoning in this paper still a 2D representation is chosen, but the wave field extrapolation inside and outside the circular area is avoided. This means that the wave field analysis is limited to the Fourier series angular coefficients  $\dot{P}_v(\omega, \rho)$  instead of the circular harmonic coefficients  $C_v(\omega)$ . Actually the former ones are not radius independent, but they still provide the required spatial resolution information. In the following examples the desired, theoretical, and measured sound fields are expressed in terms of their Fourier series angular coefficients.

## 2.4 Wave Field Representations

### 2.4.1 Desired Wave Field.

The term desired wave field or target wave field indicates the analytic description of a wave field to be reproduced by means of any of the above mentioned rendering techniques. The Fourier series angular coefficients of the desired sound field can be obtained directly from the given analytic description. Consider the example of a plane wave from the direction  $\phi_0$

$$P(\omega, \rho, \phi) = P(\omega) e^{jk\rho \cos(\phi_0 - \phi)}. \quad (3)$$

Expanding into a Fourier series w.r.t.  $\phi$  gives the well-known Jacobi-Anger expansion [7]

$$P(\omega, \rho, \phi) = \sum_{v=-\infty}^{\infty} j^v P(\omega) e^{-jv\phi_0} J_v(k\rho) e^{jv\phi}, \quad (4)$$

where the comparison with (2) shows that

$$\dot{P}_v(\omega, \rho) = j^v P(\omega) e^{-jv\phi_0} J_v(k\rho). \quad (5)$$

The analytic expression of the angular Fourier coefficients may be not straightforward in some cases, nevertheless it is always possible to obtain the value of the coefficients numerically by computing the fast Fourier transform of the target wave field with respect to the angle  $\phi$  for a given radius  $\rho_0$ . This procedure is described for example in [8].

### 2.4.2 Theoretical Wave Field.

The term theoretical wave field indicates the analytic description of a field produced by a number of loudspeakers at positions  $\mathbf{p}_i$  as shown in Fig. 1. Different rendering techniques may produce different theoretical wave fields which approximate the same desired wave field. The Fourier series angular coefficients follow in a similar way as for the desired wave field by expanding the sound field produced by each loudspeaker into its individual angular coefficients and superimposing all loudspeakers. The loudspeakers may be modelled as point sources unless a more elaborate loudspeaker model is available.

### 2.4.3 Measured Wave Field.

For real wave fields the Fourier series angular coefficients can be obtained directly from measurements on a circle of radius  $\rho_0$ . The integral for the determination of the Fourier coefficients is approximated by a DFT with respect to the azimuthal angle  $\phi$ . Thus wave fields of different nature can be compared to each other directly on the basis of their respective coefficients  $\dot{P}_v(\omega, \rho_0)$ . This procedure is shown in Sec. 4.

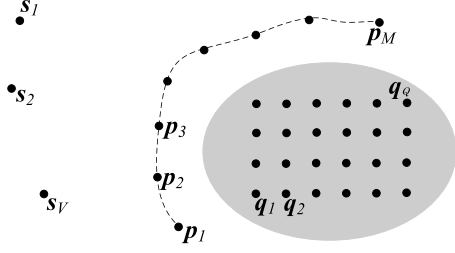


Figure 1: A very general model of a rendering system,  $s_{1,2,V}$  represent the desired virtual sources to be reproduced (see [3]).

### 3. METRICS FOR THE COMPARISON OF WAVE FIELDS

It is possible to define different error energy metrics for the comparison of wave fields. Consider two wave fields  $P(\omega, \mathbf{q})$  and  $S(\omega, \mathbf{q})$  where  $P$  is the desired wave field and  $S$  stands for any two of the theoretical or measured wave field. The space coordinate for the region of interest (grey shaded area in Fig. 1) is denoted with  $\mathbf{q}$ , where no special coordinate system is assumed yet.

A first approach resembles the idea of measuring the wave fields at many positions  $\mathbf{q}_i$ ,  $i = 1 \dots Q$  (discrete-space) and comparing the resulting signals. An actual measurement at many positions is impractical, nevertheless, such an imaginary measurement setup provides a straightforward way to the definition of a normalized error energy metrics as

$$e_d^2(\omega) = \frac{\sum_{i=1}^Q |P(\omega, \mathbf{q}_i) - S(\omega, \mathbf{q}_i)|^2}{\sum_{i=1}^Q |P(\omega, \mathbf{q}_i)|^2}, \quad (6)$$

where the normalization with respect to the energy of the whole desired wave field gives insight into the effective amount of the error. An equivalent metric is used for example in [2]. The corresponding normalized RMSE  $e_d(\omega)$  is obtained by taking the root of (6), in this way the metric is the same as presented in [3].

### 4. METRIC BASED ON FOURIER SERIES COEFFICIENTS

This section shows how to obtain an error energy metric from the Fourier series coefficients. At first an energy metric for one signal is considered, then follows the metric for the difference between two signals.

#### 4.1 Signal Energy Metric

A continuous-space energy metric is given by the following integral over the area of interest  $A$

$$W^2(\omega) = \int_A |P(\omega, \mathbf{q})|^2 d\mathbf{q}. \quad (7)$$

Expressing the space coordinate  $\mathbf{q}$  in polar coordinates, i.e.  $P(\omega, \mathbf{q}) = P(\omega, \rho, \phi)$ , the definition (7) can be refined as

$$W^2(\omega) = \frac{1}{2\pi\rho_0} \int_0^{\rho_0} \int_0^{2\pi} |P(\omega, \rho, \phi)|^2 d\rho d\phi. \quad (8)$$

This definition allows to make effective use of the circular harmonics from (2), when the region  $A$  is chosen as the interior of a circle. Its radius  $\rho_0$  does not have to correspond to the radius of any circular measurement device. However the extrapolation of three-dimensional wave fields inside the circle by means of circular harmonics poses the problems mentioned in 2.3. Therefore it is wise to consider the energy only at the fixed radius  $\rho_0$ , which has to correspond to the radius of the measurement device. Expressing  $P(\omega, \rho, \phi)$  by the Fourier coefficients similar to (2)

$$P(\omega, \rho, \phi) = \sum_{v=-\infty}^{\infty} \hat{P}_v(\omega, \rho) e^{jv\phi}, \quad (9)$$

and integrating the energy at fixed radius  $\rho_0$ , yields the following energy metric for the wave field  $P(\omega, \rho, \phi)$

$$V^2(\omega) = \frac{1}{2\pi} \int_0^{2\pi} |P(\omega, \rho_0, \phi)|^2 d\phi = \sum_v |\hat{P}_v(\omega, \rho_0)|^2. \quad (10)$$

The above expression can be thought as an energy metric relative to the radius  $\rho_0$  expressed in terms of the Fourier series angular coefficients  $\hat{P}_v(\omega, \rho_0)$ .

#### 4.2 Difference between Two Signals

The difference between two signals  $P(\omega, \mathbf{q})$  and  $S(\omega, \mathbf{q})$  can be still expressed by the respective Fourier series angular coefficients in much the same way as the energy metric for one signal in Sec. 4.1.

Refining the definition of the distance metric to the circle with radius  $\rho_0$  and considering the normalization term results in

$$e_\rho^2(\omega) = \frac{\sum_{v=-\infty}^{\infty} |\hat{P}_v(\omega, \rho_0) - \hat{S}_v(\omega, \rho_0)|^2}{\sum_{v=-\infty}^{\infty} |\hat{P}_v(\omega, \rho_0)|^2}. \quad (11)$$

The corresponding normalized RMSE  $e_\rho(\omega)$  is obtained by taking the root of (11). Within the following section the arguments are omitted for brevity and  $\hat{S}_v^T$  and  $\hat{S}_v^M$  stand for the coefficients of theoretical and measured wave fields, respectively.

## 5. EXPERIMENTAL RESULTS

### 5.1 Experimental Setup

The suitability of the above described evaluation metric is proven for the same measured data used in [3]. The measurement principle is already described there in Sec. 2 and further details are available in [8], therefore in the following only a brief description of the experimental setup is given. The setup of the experiment consists of a virtual circular microphone array and a circular loudspeaker array placed in the low-reverberation chamber of the LMS laboratory. The virtual microphone array is composed of an omnidirectional and a figure-of-eight microphone mounted on a rotating arm. A stepper motor positions the arm at 200 equally spaced positions on a circle with radius of  $\rho_0 = 0.74$  m. This rotating rig is placed at the center of the circular loudspeaker array which accommodates 48 high-quality emitters on a circle with radius 1.5 m. Fig. 2 shows the overall setup of the experiment.



Figure 2: The setup of the experiment.

## 5.2 Scaling of the Measured Data

When the measured wave field  $S^M$  is considered, an opportune scaling of the measured data is necessary in order to compensate for the microphone gains and amplifications. The scaling factor can be simply obtained by imposing that the energy of the measured coefficients equals the one of the theoretical coefficients as already discussed in [3]. This leads to the following scaling of the Fourier coefficients  $\hat{S}_v^M$

$$\bar{\hat{S}}_v^M(\omega, \rho_0) = \hat{S}_v^M(\omega, \rho_0) \frac{V^T(\omega)}{V^M(\omega)}, \quad (12)$$

with

$$V^{T,M}(\omega) = \sqrt{\sum_{v=-\infty}^{\infty} |\hat{S}_v^{T,M}(\omega, \rho_0)|^2}. \quad (13)$$

Now the distance metric in (11) can be computed for theoretical and also for measured wave fields by inserting  $\hat{S}_v^T$  or  $\bar{\hat{S}}_v^M$  in place of  $\hat{S}_v$ .

## 5.3 Comparison of the Results

This section presents the results obtained with the new metric  $e_\rho(\omega)$  along with the ones from [3] obtained with the discrete-space metric  $e_d(\omega)$  from (6). Both metrics are computed to quantify the differences between desired and theoretical wave fields, desired and measured wave fields. The chosen target wave field  $P$  for the experiment simulates a monochromatic omnidirectional point source with different frequencies  $f$  and distances  $d$  from the array center. As in [3] two different rendering techniques are evaluated, namely Wave Field Synthesis (WFS) [13] and Geometric Rendering (GR) [14].

Tab. 1 and Tab. 2 show theoretical and experimental results of the evaluation, respectively. In both cases the metrics  $e_d(\omega)$  and  $e_\rho(\omega)$  show that GR slightly outperforms WFS at high temporal frequencies. On the other hand the new metric expressed in the angular frequency domain tends to give better scoring to WFS at low temporal frequencies. This fact may be further investigated by generalizing the metric as shown in the next section.

Table 1: Evaluation metrics computed for the difference between desired and theoretical wave fields. Best performances are emphasized in bold fonts for the new metric  $e_\rho(\omega)$ .

| $f$ [Hz] | $d$ [m] | WFS           |                  | GR            |                  |
|----------|---------|---------------|------------------|---------------|------------------|
|          |         | $e_d(\omega)$ | $e_\rho(\omega)$ | $e_d(\omega)$ | $e_\rho(\omega)$ |
| 500      | 3 m     | 0.235         | <b>0.099</b>     | 0.221         | 0.174            |
| 500      | 6 m     | 0.271         | <b>0.202</b>     | 0.271         | 0.216            |
| 500      | 10 m    | 0.300         | 0.247            | 0.228         | <b>0.232</b>     |
| 1000     | 3 m     | 0.296         | <b>0.108</b>     | 0.241         | 0.183            |
| 1000     | 6 m     | 0.312         | <b>0.204</b>     | 0.288         | 0.222            |
| 1000     | 10 m    | 0.334         | 0.247            | 0.304         | <b>0.236</b>     |
| 1500     | 3 m     | 0.792         | 0.663            | 0.498         | <b>0.661</b>     |
| 1500     | 6 m     | 0.689         | 0.583            | 0.520         | <b>0.499</b>     |
| 1500     | 10 m    | 0.675         | 0.568            | 0.593         | <b>0.500</b>     |

Table 2: Evaluation metrics computed for the difference between desired and measured wave fields. Best performances are emphasized in bold fonts for the new metric  $e_\rho(\omega)$ .

| $f$ [Hz] | $d$ [m] | WFS           |                  | GR            |                  |
|----------|---------|---------------|------------------|---------------|------------------|
|          |         | $e_d(\omega)$ | $e_\rho(\omega)$ | $e_d(\omega)$ | $e_\rho(\omega)$ |
| 500      | 3 m     | 0.502         | <b>0.400</b>     | 0.503         | 0.428            |
| 500      | 6 m     | 0.506         | 0.428            | 0.455         | <b>0.417</b>     |
| 500      | 10 m    | 0.446         | 0.436            | 0.453         | <b>0.431</b>     |
| 1000     | 3 m     | 0.753         | 0.548            | 0.680         | <b>0.522</b>     |
| 1000     | 6 m     | 0.613         | 0.559            | 0.603         | <b>0.558</b>     |
| 1000     | 10 m    | 0.593         | 0.578            | 0.587         | <b>0.571</b>     |
| 1500     | 3 m     | 1.043         | 0.919            | 0.731         | <b>0.742</b>     |
| 1500     | 6 m     | 0.863         | 0.842            | 0.700         | <b>0.699</b>     |
| 1500     | 10 m    | 0.898         | 0.845            | 0.728         | <b>0.694</b>     |

## 5.4 Generalization of the Metric

To make the metric more flexible and expressive it is possible to consider a weighting function  $G_v(\omega)$  which restricts the evaluation to a specific region of angular and temporal frequencies of interest. Then the metric (11) adopts the more general form

$$E_\rho^2 = \frac{\int_0^\infty \sum_{v=-\infty}^{\infty} G_v(\omega) |\hat{P}_v(\omega, \rho_0) - \hat{S}_v(\omega, \rho_0)|^2 d\omega}{\int_0^\infty \sum_{v=-\infty}^{\infty} G_v(\omega) |\hat{P}_v(\omega, \rho_0)|^2 d\omega}. \quad (14)$$

For example in the above presented experiment the function  $G_v(\omega)$  can be thought as three Dirac impulses each centered at one of the temporal frequencies  $f = 500, 1000, 1500$  Hz. Since the corresponding results in Tab. 1 and Tab. 2 reveal a slightly better performance of GR at high frequencies it is interesting to consider for the theoretical evaluation two specific evaluation regions, i.e.  $G_v(\omega)$  resembles a 2D rect function centered in two different positions as shown by the dashed and dotted rectangles in Fig. 3. The dotted region (550-1050 Hz) comprises a frequency range where the loudspeaker array from Fig. 2 exhibits little aliasing, while the dashed region (950-1450 Hz) is chosen to include significant aliasing effects. Note that with this generalization the error metric implicitly includes an averaging over frequencies and

restricts to low order modes. The metric is then modified as follows

$$E_{\rho}^2 = \frac{\int_{\omega_1}^{\omega_2} \sum_{-v_1}^{v_1} |\dot{P}_v(\omega, \rho_0) - \dot{S}_v(\omega, \rho_0)|^2 d\omega}{\int_{\omega_1}^{\omega_2} \sum_{-v_1}^{v_1} |\dot{P}_v(\omega, \rho_0)|^2 d\omega}, \quad (15)$$

where  $\omega_{1,2}$  determine the frequency range of interest and  $v_1$  the highest angular mode considered. The corresponding results are compiled in Tab. 3, they confirm the advantages which GR offers at high temporal frequencies whereas at low frequencies WFS still guaranties a more accurate reproduction of angular modes.

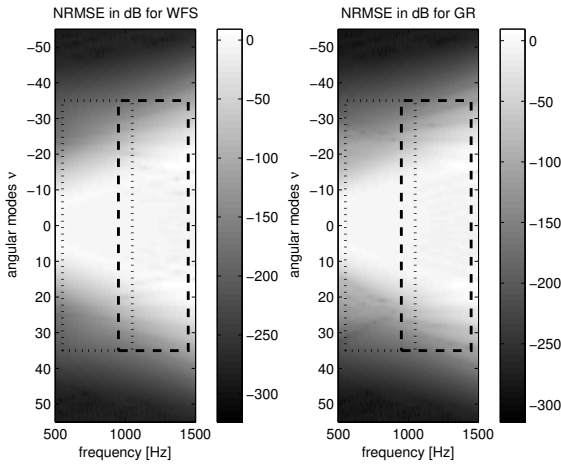


Figure 3: The figure represents the theoretical normalized RMSE in dB for each frequency  $\omega = 2\pi f$  and mode  $v$ , the dashed rectangles show the regions selected for the evaluation through the weighting function  $G_v(\omega)$ .

Table 3: Evaluation metric computed for the difference between desired and theoretical wave fields within specific regions of angular and temporal frequencies. Best results are emphasized in bold fonts.

| $f$ [Hz] | $d$ [m] | WFS          | GR           |
|----------|---------|--------------|--------------|
|          |         | $E_{\rho}$   | $E_{\rho}$   |
| 550-1050 | 3 m     | <b>0.094</b> | 0.173        |
| 550-1050 | 6 m     | <b>0.202</b> | 0.215        |
| 550-1050 | 10 m    | <b>0.224</b> | 0.230        |
| 950-1450 | 3 m     | 0.364        | <b>0.318</b> |
| 950-1450 | 6 m     | 0.395        | <b>0.363</b> |
| 950-1450 | 10 m    | 0.424        | <b>0.385</b> |

## 6. CONCLUSIONS

In this paper an alternate evaluation metric is presented which enables to compare the accuracy of different wave field rendering techniques. It relies on 2D measurements on a circle and the corresponding Fourier series angular coefficients, thus it reveals the capability of the rendering system

to reproduce the angular modes on a circle which embraces the listening area. Such a metric is simple and does not involve the wave field extrapolation inside the evaluation area. It is compared with the discrete space metric already used by the authors in [3], moreover it is extended by an additional weighting function which allows to focus on certain regions of interest in the frequency-mode-number plane. Simulations and experimental results show that the new metric allows a flexible assessment of the characteristics of the rendering techniques.

## REFERENCES

- [1] J. Ahrens, H. Wierstorf, and S. Spors, "Comparison of higher order ambisonics and wave field synthesis with respect to spatial discretization artifacts in time domain," in *Proc. of AES 40th International Conference on Spatial Audio*, Tokyo, Japan, October 2010.
- [2] G. N. Lilis, D. Angelosante, and G. B. Giannakis, "Sound field reproduction using Lasso," *IEEE Transactions on Audio, Speech, and Language Processing*, vol. 18, pp. 1902–1912, November 2010.
- [3] A. Canclini, P. Annibale, F. Antonacci, A. Sarti, R. Rabenstein, and S. Tubaro, "An evaluation of the accuracy of wave field rendering techniques based on circular harmonic decomposition," in *Proc. of 36th Int. Conference on Acoustics, Speech and Signal Processing (ICASSP)*, 2011.
- [4] A. Kuntz and R. Rabenstein, "Cardioid pattern optimization for a virtual circular microphone array," in *Proc. of EAA Symposium on Auralization*, Helsinki, 2009.
- [5] G. B. Arfken and H. J. Weber, *Mathematical Methods for Physicists*. Amsterdam: Academic Press, 2000.
- [6] F. Zotter and P. Plessas, "Microphone arrays around rigid spheres for spatial recording and holography," in *DAGA*, Berlin, March 2010.
- [7] E. Williams, *Fourier Acoustics*. London: Academic Press, 1999.
- [8] A. Kuntz, *Wave Field Analysis Using Virtual Circular Microphone Arrays*. München, Germany: Verlag Dr. Hut, 2009.
- [9] M. A. Poletti, "A unified theory of horizontal holographic sound systems," *Journal of the Audio Engineering Society*, vol. 48, pp. 1155–1182, December 2000.
- [10] H. Teutsch, *Modal Array Signal Processing: Principles and Applications of Acoustic Wavefield Decomposition*. Berlin: Springer, 2007.
- [11] T. Betlehem and T. D. Abhayapala, "Theory and design of sound field reproduction in reverberant rooms," *Journal of the Audio Engineering Society*, vol. 117, pp. 2100–2111, April 2005.
- [12] E. Hulsebos, T. Schurmanns, D. de Vries, and R. Boone, "Circular microphone array for multichannel audio recording," in *Proc. of 114th AES Convention*, Amsterdam, March 2003.
- [13] A. Berkhout, "Acoustic control by wave field synthesis," *J. Acoust. Soc. Am.*, vol. 93, pp. 2764–2778, 1993.
- [14] F. Antonacci, A. Calatroni, A. Canclini, A. Galbiati, A. Sarti, and S. Tubaro, "Soundfield rendering with loudspeaker arrays through multiple beam shaping," in *Proc. of IEEE Workshop on Applications of Signal Processing to Audio and Acoustics, WASPAA '09*, 2009.